let

Effect of vacancy defect position on the Zigzag Phosphorene Nanoribbon Tunneling FETs

Hadi Owlia, Mohammad Bagher Nasrollahnejad, and Abdalhossein Rezai

Abstract-In this paper, the important characteristics of a **Zigzag Phosphorene Nanoribbon Tunneling FET (ZPNR-TFET)** are studied by inserting a single vacancy (SV) defect. After adjusting the positions of the defect in the length of the channel, it is found that the SV defect decreases on current in all three defect positions, and the biggest reduction is when the SV defect is in the center position. The off current decreases when the SV defect is located in the center of the channel and increases when the defect is located near the source and drain. The largest increase in off current is related to the location of the defect close to the source. The on-off current ratio decreases in all three defect positions. The greatest impact is related to the condition where the defect is located on the source side. Semi-empirical Slater-Koster approach using DFTB-CP2K parameters were used for the density functional based tight binding (DFTB) calculations of ZPNR.

Keywords—Phosphorene nanoribbon; vacancy defect; CP2K method; Density functional tight binding

I. INTRODUCTION

WO-DIMENSIONAL ultrathin nanomaterials, such as

silicene [1], graphene [2], hexagonal boron nitride [3], molybdenum disulfide [4], and graphitic carbon nitride [5] have received significant attention recently due to their excellent features and possibly applications. Graphene a 2D semi-metallic nanomaterial, has outstanding electronic exclusivities, such as excellent thermal conductivity and high carrier mobility, however, the absence of bandgap restricts its performances of high on-off ratio and large off current for graphene-based nanoelectronic devices. A similar issue also exists in a silicon monolayer and silicene, which has most similar notable properties to graphene although it has a buckled honeycomb structure [1]. Very recently, black phosphorus (phosphorene) has attracted much interest because of its

Black phosphorus is the most stable allotrope of phosphorus at room temperature, which was made from white phosphorus under high pressure and temperature [6]. Black phosphorus has a layered structure and the force between the layers is of the van der Waals type, and they can be separated from the bulk structure by mechanical methods and a single-layer or multilayer structure can be made. The separated layer of black

distinctive electronic properties.

phosphorus is called phosphorene. Phosphorene has a hexagonal structure and is folded due to the presence of sp³ covalent bonds between atoms, which gives phosphorene special physical properties. Phosphorene is an intrinsic P-type semiconductor and has an acceptable energy gap of about 1eV [6]. Phosphorene has many applications in the manufacture of solar cells, batteries, transistors, sensors, energy conversion and storage.

Phosphorene also indicates some outstanding electronic properties better than silicene and graphene. FETs based on a few layers of phosphorene were found to have an on/off ratio of up 10⁵. Furthermore, it is the only stable two-dimensional nanomaterials that can be mechanically exfoliated in the experiments [7].

Despite all the excellent properties of this two dimensional ultrathin nanomaterial, the electrical properties of phosphorene can be changed by various methods, such as applying an electric field, adding other elements to the phosphorene structure, and creation of structural defects [7]. Farogh and his colleagues [8] found that by introducing a single-vacancy defect, defect-induced levels are created in the energy gap region and cross the Fermi energy line, but by introducing a double-vacancy defect, an energy gap is observed. Sreostava and his colleagues [9] showed that by introducing a single-vacancy defect in phosphorene, defect-induced states are created in the energy gap, which causes the sample to exhibit magnetic properties. However, by introducing a double-vacancy defect, the sample no longer has magnetic properties.

These structural defects are unavoidably present in silicene and graphene and strictly affect their electronic and structural properties and it has been investigated in various papers [10-16]. However, until now, the investigation of defects in phosphorene has received less attention. There are various defects in phosphorene because it has a low symmetry lattice. Moreover, Defects are easily formed in phosphorene compared to silicone and graphene [17]. Defects with dissimilar structures reveal dissimilar stability and electronic properties.

At temperature T, the areal defect density of N_{Defect} (m⁻²) in 2D nanomaterials obtained by the Arrhenius formula [17]

$$N_{defect} = N_{conv} \cdot EXP(-E_f/K_BT) \tag{1}$$

Where N_{conv} is the areal density of atoms in conventional 2D nanomaterials, $E_{\rm f}$ is the formation energy of a defect created in



H. Owlia is assistant professor at Department of Electrical Engineering, Faculty of Engineering, Ardakan University, P.O. Box 184, Ardakan, Iran (e-mail: howlia@ardakan.ac.ir).

M.B. Nasrollahnejad is assistant professor at Department of Electrical Engineering, Gorgan Branch, Islamic Azad University, Gorgan, Iran (e-mail: MB.Nasrollahnejad@iau.ac.ir).

A. Rezai is associate professor at Department of Electrical Engineering, University of Science and Culture, Tehran, Iran (e-mail: rezai@usc.ac.ir).

2 H. OWLIA, ET AL.

nanomaterials and k_B is the Boltzmann constant. For conventional graphene, phosphorene and silicene, areal densities are $3.79\times10^{19}~m^{-2}$, $2.62\times10^{19}~m^{-2}$ and $1.55\times10^{19}~m^{-2}$, respectively. By calculating the areal density, we find that structural defects have a much higher areal density in phosphorene and they are much simply created in phosphorene structures.

In this paper, for the first time, the effect of vacancy defect position on the phosphorene nanoribbon tunneling FETs is investigated. The reason for using the tunnel structure in this work is that tunneling field-effect transistors (TFETs) are suitable for designing circuits with low power dissipation. The rest of the paper is organized as follows: The device configuration and computational method are discussed in section 2. Section 3 deals with simulation results. Finally, important results are summarized in section 4.

II. DEVICE CONFIGURATION AND COMPUTATIONAL METHOD

The PNR-TFET[18] shown in Fig. 1 characterizes a structure that phosphorene nanoribbons with a zigzag edge (ZPNR) serving as the channel material, and the ZPNR layer sandwiched between two oxide layers (dielectric constant is 3.9). Equivalent oxide thickness (EOT) is 0.5 nm. The ZPNR has particular channel widths and lengths of 2.3 nm and 3.3 nm, respectively. This geometric configuration comforts control of current flow and effective charge carrier tunneling. The channel is assumed to be intrinsic. Two gate terminals modulate the tunneling of carriers. The source and drain regions are doped with doping concentrations of 3×10^{10} cm⁻² and -5×10^{11} cm⁻², respectively.

For modeling and analyzing the electronic properties of phosphorene, a precise definition of the system's Hamiltonian is required. We use the CP2K software package for this purpose. In CP2K, the Hamiltonian has an important role in

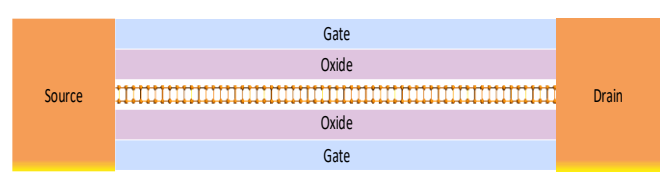


Fig.1. Schematic diagram of a ZPNR-TFET.

describing the dynamics of the system being investigated. CP2K is an open-source molecular dynamics and electronic structure software package to perform atomistic simulations of molecular, liquid, solid-state, and biological systems [19].

In CP2K software, the computational methods are semiempirical (SE) models based on the density functional-based tight-binding methods (DFTB) [20]. CP2K utilizes DFTB as one of its computational methods for studying the electronic structure of systems [21]. DFTB (Density Functional Tight Binding) is a method that approximates DFT calculations by simplifying the electronic structure calculations. Most of the applications with CP2K are based on the Kohn–Sham (KS) based DFT-GGA approach [22]. In the context of DFTB, the Hamiltonian is modified to include terms that capture the electronic structure of the system using a set of empirical parameters.

Electronic kinetic energy T, nuclear potential energy V_{nuc} (involves the interaction of electrons with the phosphorus

nuclei), and electronic potential energy $V_{\rm elec}$ (includes the external potential and electron-electron interaction) are constituents of the Hamiltonian. The total Hamiltonian for phosphorene is defined as:

$$H = T + V_{elec} + V_{nuc} \tag{2}$$

The total Hamiltonian can be used to create the Green's function for further analysis [23-24]. The retarded/advanced Green's function in NEGF is defined as:

$$G^{r/a} = (EI - H - \sum_{S} - \sum_{D})^{-1}$$
 (3)

that Σ_S and Σ_D are the self-energy matrices for the source and drain contacts.

For determining the electrostatic potential within this structure as influenced by the charge distribution, we use the Poisson equation self-consistently within the NEGF formalism [25-33].

In this paper, a density mesh cut-off of 150 Ry is used, and a 1x1x16 Monkhorst-Pack k-point sampling is applied for nanodevice simulation. Computations are carried out at a temperature of T=300 K. Atomistix ToolKit (ATK) package is applied for the simulation, including the aforementioned parameters. The transmission coefficient $T(E, k_x)$ for a given k_x and energy E can be defined as[34-42]:

$$T(E, k_x) = Tr[G^r(E, k_x). \Gamma_S(E, k_x). G^a(E, k_x). \Gamma_D(E, k_x)]$$
(4)

and

$$\Gamma_{S/D}(E, k_x) = i \left(\sum_{S/D}^{r} (E, k_x) - \sum_{S/D}^{a} (E, k_x) \right)$$
(5)

is the broadening of contacts, that

$$\sum_{S/D}^{r/a} (E, k_{\chi}) \tag{6}$$

are self-energies matrices. The electrical current is calculated using the Landauer–Buttiker relation [25].

$$I = \int J(E)dE \tag{7}$$

that J(E) is known as the energy-resolved current spectrum and is defined as follows.

$$J(E) = \frac{2q}{h} [f(E - E_{FS}) - f(E - E_{FD})T_r(E)]$$
 (8)

in which $T_r(E)$ is transmission at a definite energy level and $E_{FS/D}$ is the Fermi energy in contact.

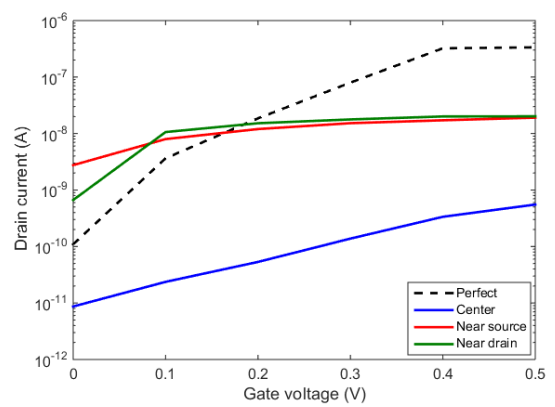
III. RESULTS AND DISCUSSIONS

Fig. 2 compares the transfer characteristics of the ideal structure with the defected structures which the single vacancy defects are in three positions along the channel length.

As shown, the off current decreases when the SV defect is located in the center of the channel and increases when the defect is located near the source and drain, the largest increase in off current is related to the location of the defect close to the source. However, on current is reduced in all three cases which

3

is the biggest decrease related to the case where the defect is located in the center of the channel. On current is almost equal when the defect is close to the source and drain contacts. The reason for the increase in device current with increasing gate voltage is that the difference between the channel Fermi level and the Fermi level of the contacts changes with gate voltage



changes in phosphorene, and it moves the amount of local

Fig.2. I_D - V_G characteristics for the ZPNR-TFET and defected ZPNR-TFET at different defect positions at V_D = 0.5 V_\cdot

density of states profile (LDOS) up or down in the channel region. To better analyze the carrier transport behavior when carriers travel throughout the ZPNR channel, the LDOS profile is investigated in this paper. Fig. 3 exhibits the LDOS profile at the OFF state for the ZPNR-TFET in perfect and three defected structures. When the gate voltage is zero, the electron transfer range falls in the middle of the bandgap, and the bandgap prevents the transfer of carriers to the drain side. As shown, the bandgap increases when the SV defect is located in the center of the channel, and as a result band-to-band tunneling decreases which leads to a reduction in the off current (as shown in Fig.2). Figure 4 depicts the LDOS profile in perfect and three defected structures for the ON state. When the gate voltage increases, the conduction band edge shifts to the lower energies, and the carrier transmission is placed in the conduction region of the channel. As the number of states increases, more electrons transfer from the source side to the drain side, and as a result, the current increases. Moreover, defects perturb the local density of state sharing in the subbands of the conduction band [10] and the regions with SV defect generate localized states which trap carriers in the transmission path [24] which leads to a reduction in the capacity of carriers transport and finally lead to a decrease in electric current.

The energy-resolved current spectrum for all structures is shown in Fig. 5 and Fig. 6 for off and on states, respectively. The area under this diagram is proportional to the amount of the drain current. As shown in Fig. 5, in the case where the defect is in the center position, the area under the diagram is the smallest. Off current increases as the area becomes larger, this is consistent with the results of Figure 2. The diagram of Figure

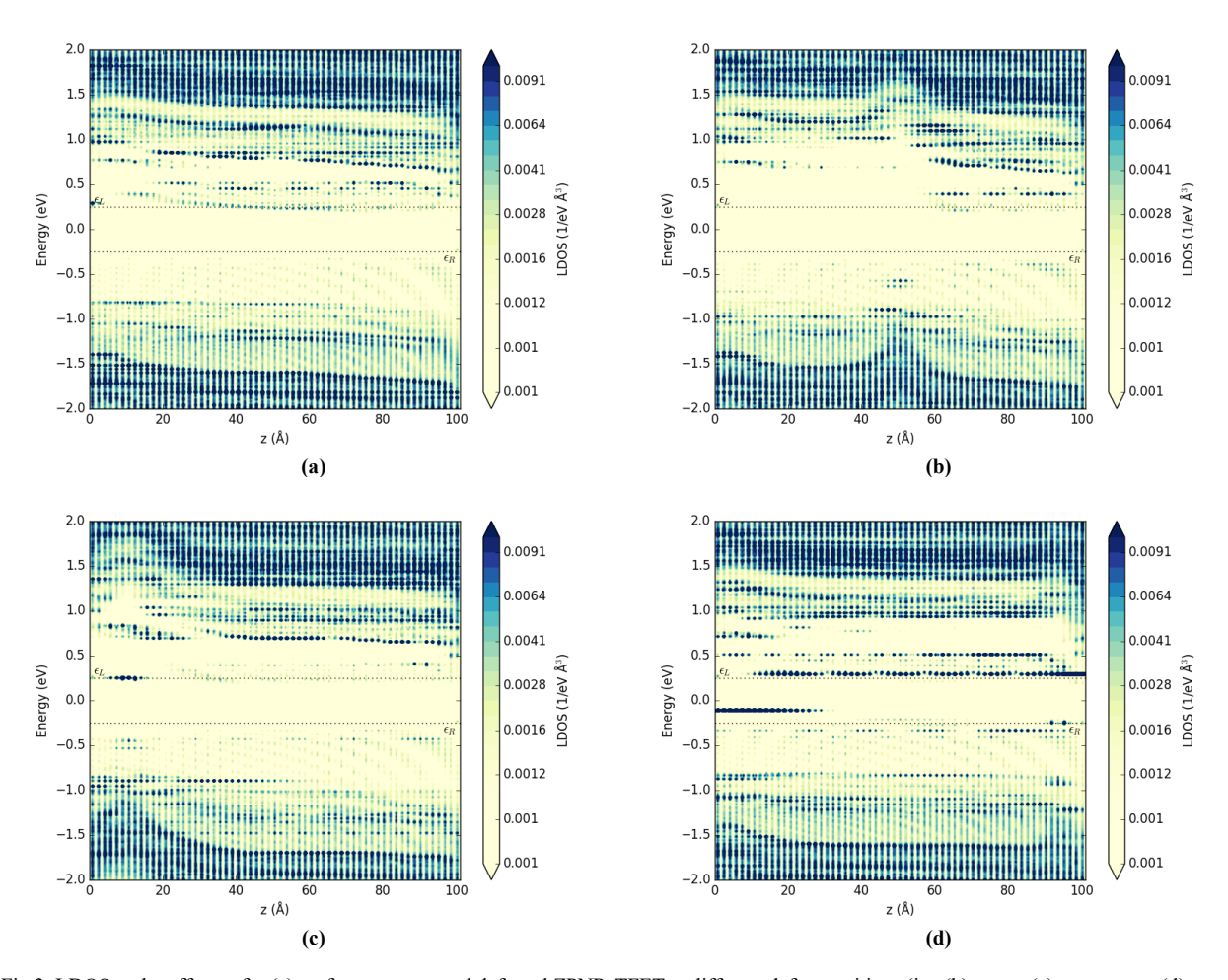


Fig.3. LDOS at the off state for (a) perfect structure and defected ZPNR-TFET at different defect positions (i.e. (b) center (c) near source (d) near drain.

H. OWLIA, ET AL.

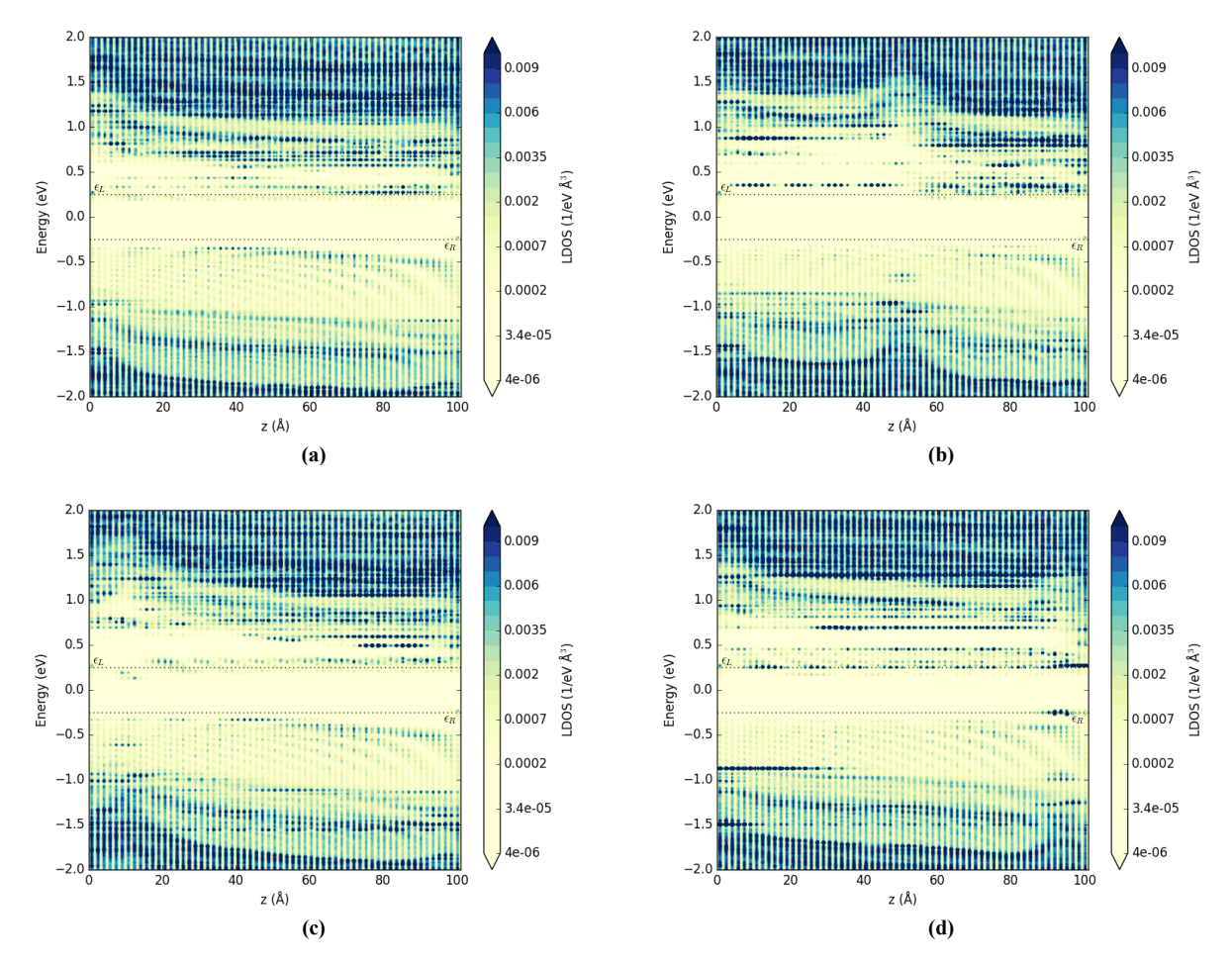


Fig.4. LDOS at the ON state for (a) perfect structure and defected ZPNR-TFET at different defect positions (i.e. (b) center (c) near source (d) near drain.

6 also confirms the results of Figure 2 in the state of on current. The perfect structure has the highest area under the diagram and the lowest value is related to the defect position in the center. This defect position also has the lowest value of ON current according to Figure 2.

The diagram of the on-off current ratio is shown in Figure 7, as can be seen in all three defect positions, this ratio decreases, and the greatest impact is related to the condition where the defect is located on the source side. The significant reduction of the on-off current ratio in this state is due to the significant increase of the off-state current in this state.

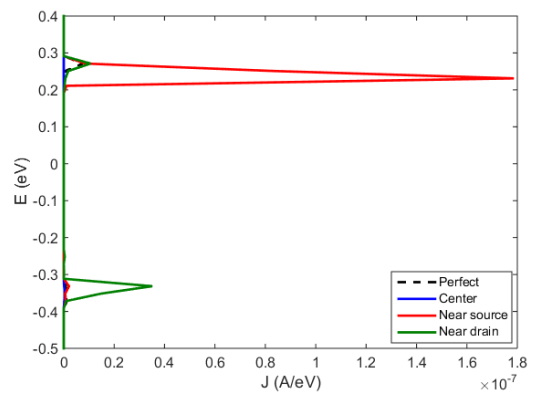


Fig. 5. Energy-resolved current spectrum $J(\mbox{\ensuremath{A/eV}})$ at OFF state.

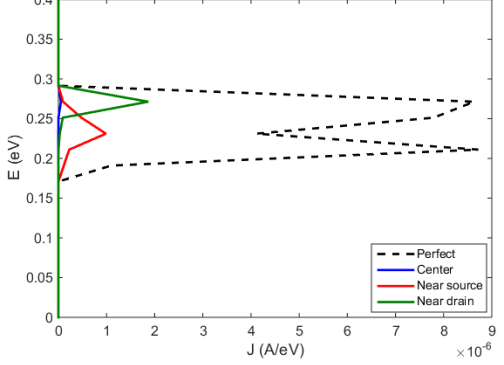


Fig. 6. energy-resolved current spectrum J(A/eV) at ON states.

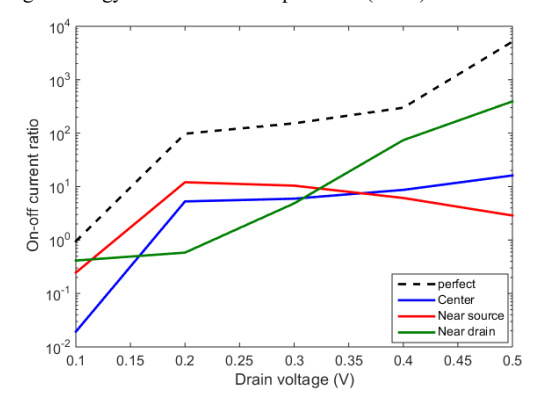


Fig. 7. On-off current ratio.

CONCLUSION

We have investigated the effect of vacancy defect position on the Zigzag Phosphorene Nanoribbon Tunneling FETs. Results reveal that the SV defect decreases on-current in all three defect positions which is the biggest decrease related to the case where the defect is located in the center of the channel. The reduction of on-current is because these defects perturb the local density of state sharing in the subbands of the conduction band and the regions with SV defect along the channel generate localized states that trap carriers in the transmission path. The off current decreases when the SV defect is located in the center of the channel and increases when the defect is located near the source and drain. The highest off-current value is when the defect is on the source side. The on-off current ratio decreases in all three defect positions. The lowest value of the on-off current ratio corresponds to when the defect is on the source side. The investigation of SV defects demonstrates a notable influence on the electrical properties of the ZPNR-TFET. As defects are inherent to manufacturing processes, this research highlights the potential of SV defects to significantly degrade the reliability of such devices.

REFERENCES

- [1] C. Grazianetti, E. Cinquanta, and A. Molle, "Two-dimensional silicon: the advent of silicone," 2D Materials, vol. 3, no.1, p.012001. 2016. https://doi.org/10.1088/2053-1583/3/1/012001
- [2] E. Galvagno, E. Tartaglia, M. Stratigaki, C. Tossi, L. Marasco, F. Menegazzo, C. anardi, F. Omenetto, C. Coletti, A. Traviglia, and M. Moglianetti, "Present Status and Perspectives of Graphene and graphene-related Materials in Cultural Heritage," *Advanced Functional Materials*, vol. 34, no.13, p.2313043, 2024. https://doi.org/10.1002/adfm.202313043
 [3] S. Roy, X. Zhang, A.B. Puthirath, A. Meiyazhagan, S. Bhattacharyya, M.M. Rahman, G. Babu, S. Susarla, S.K. Saju, M.K. Tran, and L.M. Sassi, "Structure, properties and applications of two-dimensional hexagonal boron nitride," *Advanced Materials*, vol. 33, no.44, p.2101589, 2021. https://doi.org/10.1002/adma.202101589
- [4] O. Samy, S. Zeng, M.D. Birowosuto, and A. El Moutaouakil, "A review on MoS2 properties, synthesis, sensing applications and challenges," *Crystals*, vol. 11, no.4, p.355. 2021. https://doi.org/10.3390/cryst11040355

 [5] N. Rono, J.K. Kibet, B.S. Martincigh, and V.O. Nyamori, "A review of
- the current status of graphitic carbon nitride," *Critical Reviews in Solid State and Materials Sciences*, vol. 46, no.3, pp.189-217.2021. https://doi.org/10.1080/10408436.2019.1709414
- [6] W. Zhang, X. Zhang, L.K. Ono, Y. Qi, and H. Oughaddou, "Recent advances in phosphorene: structure, synthesis, and properties," *Small*, vol. 20, no.4, p.2303115. 2024. https://doi.org/10.1002/smll.202303115
- [7] L. Ding, P. Shao, Y. Yin, and F. Ding," Synthesis of 2D Phosphorene: Current Status and Challenges," *Advanced Functional Materials*, p.2316612, 2024. https://doi.org/10.1002/adfm.202316612
- [8] M. U. Farooq, A. Hashemi, J. Hong," Anisotropic bias dependent transport property of defective phosphorene layer," *Scientific Reports* 5(1) 12482, 2015. https://doi.org/10.1038/srep12482
- [9] P.Srivastava, K.P.S.S.Hembram, H.Mizuseki, K.R.Lee, S.S. Han, S. Kim, "Tuning the Electronic and Magnetic Properties of Phosphorene by Vacancies and Adatoms," J. Phys. Chem. C 119, pp. 6530–6538, 2015. https://doi.org/10.1021/jp5110938
- [10] M.B. Nasrollahnejad, and P. Keshavarzi, "Inverse Stone Throwers Wales defect and enhancing ION/IOFF ratio and subthreshold swing of GNR transistors," *The European Physical Journal Applied Physics*, vol. 86, no.2, p.20202.July2019. https://doi.org/10.1051/epjap/2019190033
- [11]H. Owlia, "Effects of passivation type on electrical transport of a defectengineered graphene nanoribbon FET," *Journal of Computational Electronics*, vol. 22, no. 2, pp.626-633, 2023. https://doi.org/10.1007/s10825-023-02009-9

- [12] M.B. Nasrollahnejad, and P. Keshavarzi, "Inverse Stone-Thrower-Wales defect and transport properties of 9AGNR double-gate graphene nanoribbon FETs," *Journal of Central South University*, vol. 26, no.11, pp.2943-2952, 2019.https://doi.org/10.1007/s11771-019-4226-0
- [13]H. Owlia, P. Keshavarzi, and M.B. Nasrollahnejad, "Effects of Stone-Wales defect position in graphene nanoribbon field-effect transistor," *J. Nano Electr. Phys.* Vol.9,no. 6, p. 06008, 2017. https://doi.org/10.21272/jnep.9(6).06008
- https://doi.org/10.21272/jnep.9(6).06008
 [14]H. Owlia, and P. Keshavarzi, "Locally defect-engineered graphene nanoribbon field-effect transistor." *IEEE Transactions on Electron Devices*, vol. 63, no.9, pp.3769-3775. 2016. https://doi.org/10.1109/TED.2016.2594777
- [15] J. Gao, J., Zhang, H. Liu, Q. Zhang, and J. Zhao, "Structures, mobilities, electronic and magnetic properties of point defects in silicone," *Nanoscale*, vol. 5, no. 20, pp.9785-9792, 2013. https://doi.org/10.1039/C3NR02826G
- [16] F. Wan, X. Wang, Y. Guo, J. Zhang, Z. Wen, and Y. Li, "Role of line defect in the bandgap and transport properties of silicene nanoribbons," *Physical Review B*, vol.104, no.19, p.195413,2021. https://doi.org/10.1103/PhysRevB.104.195413
- [17] W. Hu, and J. Yang, "Defects in phosphorene," *The Journal of Physical Chemistry C*, vol. 119, no. 35, pp.20474-20480, 2015. https://doi.org/10.1021/acs.jpcc.5b06077
- [18]H. Owlia, and M.B. Nasrollahnejad, "Exploring performance characteristics via edge configuration in black phosphorene TFETs," *International Journal of Modern Physics B*, p.2540048, 2024. https://doi.org/10.1142/S021797922540048X
- [19] T.D. Kühne, M. Iannuzzi, M. Del Ben, V.V. Rybkin, P. Seewald, F. Stein, T. Laino, R.Z. Khaliullin, O. Schütt, F. Schiffmann, and D. Golze, "CP2K: An electronic structure and molecular dynamics software package-Quickstep: Efficient and accurate electronic structure calculations," *The Journal of Chemical Physics*, vol. 152, no.19, 2020. https://doi.org/10.1063/5.0007045
- [20] G. Murdachaew, CJ. Mundy, GK. Schenter, T. Laino, and J. Hutter, "Semiempirical Self-Consistent Polarization Description of Bulk Water, the Liquid-Vapor Interface, and Cubic Ice," J Phys Chem A, vol.115, no. 23, pp. 6046–6053, 2011. https://doi.org/10.1021/jp110481m
- [21] The CP2K simulation package, https://www.cp2k.org. Accessed 20 April [22] RG. Parr, W. Yang, "Density-Functional Theory of Atoms and Molecules," Oxford University Press, Oxford, 1995.

https://doi.org/10.1093/oso/9780195092769.001.0001

- [23] H. Owlia, and P. Keshavarzi, "A bilayer graphene nanoribbon field-effect transistor with a dual-material gate," *Materials Science in Semiconductor Processing*, 39, pp.636-640, 2015. https://doi.org/10.1016/j.mssp.2015.06.014
- [24]H. Owlia, and R. Fazli, "Bilayer graphene nanoribbon field-effect transistor with electrically embedded source-side gate," *Superlattices and Microstructures*, vol. 142, p.106525, 2020. https://doi.org/10.1016/j.spmi.2020.106525
- [25] H. Owlia, M.B. Nasrollahnejad, and R. Fazli, "Phosphorene nanoribbon field effect transistor with a dual material gate," *Engineering Research Express*, vol.6, no. 2, pp. 025362(1-10), 2024. https://doi.org/10.1088/2631-8695/ad5929
- [26] T. Radsar, H. Khalesi, and V.Ghods, "Graphene nanoribbon field effect transistors analysis and applications," Superlattices and Microstructures, vol. 153, p.106869, 2021. https://doi.org/10.1016/j.spmi.2021.106869
- [27] R.K. Vobulapuram, J.B., Shaik, P. Venkatramana, D.P. Mekala, and U. Lingayath, "Design of bilayer graphene nanoribbon tunnel field effect transistor," *Circuit World*, vol. 49, no. 2, pp.174-179, 2023. https://doi.org/10.1108/CW-05-2020-0079
- [28] J.H. Hur, "The Parametric Study of Armchair Graphene Nanoribbon Field Effect Transistor by Non-Equilibrium Green's Function Method," *Journal of Nanoscience and Nanotechnology*, vol. 20, no. 8, pp.4832-4838, 2020. https://doi.org/10.1166/jnn.2020.17797
- [29] M. Hu, Z. Yang, W. Zhou, A. Li, J. Pan, and F. Ouyang, "Field effect transistors based on phosphorene nanoribbon with selective edgeadsorption: a first-principles study," *Physica E: Low-dimensional Systems and Nanostructures*, vol. 98, pp.60-65, 2018. https://doi.org/10.1016/j.physe.2017.12.027
- [30]H. Shamloo, and A.Y. Goharrizi, "Performance study of tunneling field effect transistors based on the graphene and phosphorene nanoribbons," *Micro and Nanostructures*, vol. 169, p.207336, 2022. https://doi.org/10.1016/j.micrna.2022.207336
- [31]M.K. Anvarifard, Z. Ramezani, and S.A. Ghoreishi, "A ballistic transport nanodevice based on graphene nanoribbon FET by enhanced

6 H. OWLIA, ET AL.

productivity for both low-voltage and radio-frequency scopes," *ECS Journal of Solid State Science and Technology*, vol. 11, no.6, p.061008, 2022. https://doi.org/10.1149/2162-8777/ac77ba

- [32] S.S. Ghoreishi, and R. Yousefi, "A computational study of a novel graphene nanoribbon field effect transistor," *International Journal of Modern Physics B*, vol. 31, no. 9, p.1750056, 2017. https://doi.org/10.1142/S0217979217500564
- [33]G. Liang, N. Neophytou, M.S. Lundstrom, and D.E. Nikonov, "Computational study of double-gate graphene nano-ribbon transistors," *Journal of Computational Electronics*, vol. 7, pp.394-397, 2008. https://doi.org/10.1007/s10825-008-0243-1
- [34] M.A., Hasan, S.S. Nishat, M. Hossain, and S. Islam, "Influence of Device Parameters on Performance of Ultra-Scaled Graphene Nanoribbon Field Effect Transistor," *ECS Journal of Solid State Science and Technology*, vol. 9, no. 12, p.121006, 2020. https://doi.org/10.1149/2162-8777/abce01
- [35] S.H. Dinh, H.M. Le, and T.L. Nguyen, "Graphene nanoribbon field effect transistor for digital IC application," *Journal of Technical Education Science*, vol. 15, no. 4, pp.63-68, 2020.
- [36] A. Naderi," Double gate graphene nanoribbon field effect transistor with single halo pocket in channel region," *Superlattices and Microstructures*, vol. 89, pp.170-178, 2016. https://doi.org/10.1016/j.spmi.2015.11.005
- [37] E. Suhendi, L. Hasanah, D. Rusdiana, F.A. Noor, and N. Kurniasih, "Comparison of tunneling currents in graphene nanoribbon tunnel field

- effect transistors calculated using Dirac-like equation and Schrödinger's equation," *Journal of Semiconductors*, vol. 40, no. 6, p.062002, 2019. https://doi.org/10.1088/1674-4926/40/6/062002
- [38] H. Sarvari, C. Liu, A.H. Ghayour, P. Shenavar, Z. Chen, and R. Ghayour, "Atomistic quantum transport simulation of multilayer phosphorene nanoribbon field effect transistors," *Physica E: Low-dimensional Systems and Nanostructures*, vol. 91, pp.161-168, 2017. https://doi.org/10.1016/j.physe.2017.04.015
- [39] H. Shamloo, and A.Y. Goharrizi, "Performance study of tunneling field effect transistors based on the graphene and phosphorene nanoribbons," *Micro and Nanostructures*, vol. 169, p.207336, 2022. https://doi.org/10.1016/j.micrna.2022.207336
- [40] M. Hu, Z. Yang, W. Zhou, A. Li, J. Pan, and F. Ouyang, "Field effect transistors based on phosphorene nanoribbon with selective edgeadsorption: a first-principles study," *Physica E: Low-dimensional Systems and Nanostructures*, vol. 98, pp.60-65, 2018. https://doi.org/10.1016/j.physe.2017.12.027
- [41] Poljak, M. and Suligoj, T.," The potential of phosphorene nanoribbons as channel material for ultrascaled transistors," *IEEE transactions on electron devices*, vol. 65, no. 1, pp.290-294, 2017. https://doi.org/10.1109/TED.2017.2771345
- [42] C.A. Pantis-Simut, A.T. Preda, N. Filipoiu, A. Allosh, and G.A. Nemnes, "Electric-field control in phosphorene-based heterostructures," *Nanomaterials*, vol. 12, no. 20, p.3650, 2022. https://doi.org/10.3390/nano12203650